

## AERODYNAMIC PERFORMANCE ANALYSIS OF A LOW-SPEED ACROBATIC AIRPLANE BY NUMERICAL SIMULATION

Andres D. Ortiz\*, Luis E. Quiroz\*, Rodolfo A. Köck†

\*University of Concepción  
Department of Mechanical Engineering  
Edmundo Larenas 234, Barrio Universitario, Concepción, Chile  
Casilla 160-C, correo 3 Concepción  
e-mail: [aortiz@udec.cl](mailto:aortiz@udec.cl) , [lquiroz@udec.cl](mailto:lquiroz@udec.cl) , <http://www.dim.udec.cl>

†Cadetech S.A.  
Fluid-Dynamics Division  
Serrano 551 of. 208, Concepción, Chile  
e-mail: [rkock@cadetech.cl](mailto:rkock@cadetech.cl) , <http://www.cadetech.cl>

**Keywords:** numerical, simulation, acrobatic airplane, aerodynamic, performance, analysis, FLUENT® code.

**Abstract.** *The goal of this work is to simulate and to analyze, by means of the CFD commercial code FLUENT®, the flow around a low-speed acrobatic airplane, the ENAER T-35 PILLAN, with similar characteristics to the most light civil airplanes, widely used anywhere in the world. Specifically, the aerodynamic loads on the structure are required, specifying the critical conditions of flight and the consequent load distributions on the airplane according to the application of norm FAR-23. Finally, the worst flight conditions happen at the cruise speed (Mach 0.25) and maximum load factor. In this condition the lift and drag forces, bending and torsion moments at the main spar of the wing are maximum, even greater than for the highest speed of flight (Mach 0.37). Finally, a series of graphs were made to considering the maximum loads on the wing as function of the speed of flight and the angle of attack.*

## 1 NOMENCLATURE

### 1.1 General symbols

AR	Aspect Ratio, dimensionless.
b	Wing span, m
$c_l$	Airfoil lift coefficient, dimensionless.
$C_L'$	Wing-section lift coefficient, dimensionless.
$C_{L \text{ wing}}$	Wing lift coefficient, dimensionless.
$C_{D \text{ wing}}$	Wing drag coefficient, dimensionless.
$C_p$	Pressure coefficient, dimensionless.
D	Drag force, N.
L	Lift force, N.
LA	Length of Airplane, m.
M	Mach Number, dimensionless.
$M_{t \text{ SPAR}}$	Torsion moment at the main spar, Nm.
n	Load factor, dimensionless.
V	Flight velocity, m/s.
y	Position on the wing span, m.
W	Weight of Airplane, kg.

### 1.2 Greek symbols

$\alpha$	Angle of attack, deg.
$\sigma$	Standard deviation.

## 2 INTRODUCTION

From the development of the first powered flights (1903) to the present time, the study of the aerodynamic design has played an important role in the airplanes optimization. Traditionally it has been in the hands of the designer's experience, tests of flight and wind tunnel experiments, being this last tool the one that has provided a method of systematic study and the capability of making inexpensive adjustments of control parameters in a design. At the present time, Computational Fluid Dynamics (CFD) has come to complement the experimental studying, reducing the cost in tests and time for the generation of prototypes. In this case, to study the aerodynamic properties of a constructed and designed airplane from more than 20 years, of which one stands out: cruise speed Mach 0.25, maximum Mach 0.37, load factor from 3 to +6 and weight of 2,900 lb.

With the objective of analyzing the aerodynamic performance of the airplane, a CFD model was created that allowed to make a detailed study of the loads on the main external structural elements. This way, the modeling of the flow is marked by three stages: the simulation of the flat or bidimensional flow on an airfoil, the simulation of the flow over the complete wing and

the modeling of the complete structure of the airplane, using a personal computer with a single processor, showing that this alternative was inexpensive and faster in the process of numerical calculation of the solution.

At this moment it is not within the reach of this study to innovate in the aerodynamic design, but rather to appreciate the use of this CFD code in the analysis of the aerodynamic properties of a low-speed acrobatic airplane, in this case, the current Chilean Air Force military airplane used for basic training, the ENAER T-35 Pillan (see figure1).



Figure 1. ENAER T-35 Pillan

### 3 COMPUTATIONAL GEOMETRIC MODELING

In order to obtain a detailed model that allows to calculate the loads on the diverse components of the airplane (wing/body/tail) thought was given to divide the process in three computational models or three modeling stages:

- 1) Modeling of the flat flow on the airfoil of the wing (NACA 65<sub>2</sub>-415).
- 2) Modeling of the 3D wing without fuselage.
- 3) Modeling of the simplified configuration of the airplane.

For all these stages the same boundary conditions were used: pressure far-field (PFF) at the outer contour of the domain and wall (without rugosity) for the airplane skin.

The first stage helped to define the turbulence model to be used and the minimum size of the numerical domain, comparing the results of aerodynamic loads for the airfoil with the available ones in the NACA information<sup>1</sup>. Preliminary tests with some  $k-\epsilon$  models were made (Standard, Realizable and RNG) and Spalart-Allmaras (S-A) and, like other authors shown<sup>8</sup>, RNG  $k-\epsilon$  and S-A models gave the best results for fine and coarse meshes, choosing the S-A model by their simplicity (1 transport equation) and better results.

In order to determine the minimum domain-size (being this one a limiting factor due to the high computational cost associated) the polar curves were compared for different domain-sizes (drag as function of the lift, because it is the most dependent curve of the domain-size), obtaining that from a minimum distance, between the wall surface and the outer boundary condition (PFF), of 3 times the chord (usually recommend 20 times the chord<sup>6</sup>), the results remain constant for the range of speeds of flight for this airplane.

For the finite wing simulation, the certainty in the 3D results was obtained by comparing these with traditional theoretical methods for the wing lifting-line (Prandtl, Anderson and

Rasmussen-Smith methods). In order to simplify the computational model, only the symmetrical flow around the wing was modeled, generating a symmetry condition in the wing root and a fictitious section (figure 2) that replaces the fuselage effect (suggested by the wing manufacturer).

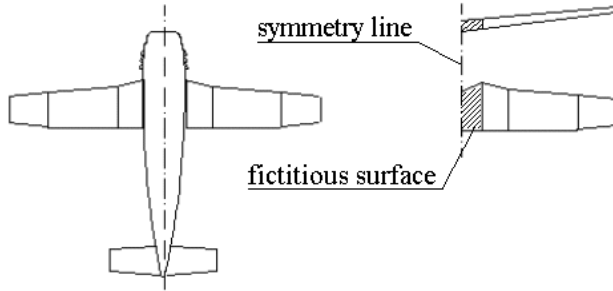


Figure 2. Finite wing model.

The model for the complete airplane (sealed, without flaps and ailerons) was thought with the same presumptions as the finite wing but under some structural simplifications such as the propeller, antennas and the flow in the engine (due to the geometric complexities and calculation in the CFD code, see fig 3) and the nose where it has been truncated so as not to diminish the drag too much. On the basis of these simplifications and other studies<sup>10-12</sup>, the drag had to be underestimated by at least 30%, a value that will have to be considered in the results. The domain-size for this model was determined from the mentioned 2D simulations. There had been included some important external forms (figure 4) like openings that were modeled like sealed shells, affecting the flow by its form and without incorporating specific boundary conditions in each case.

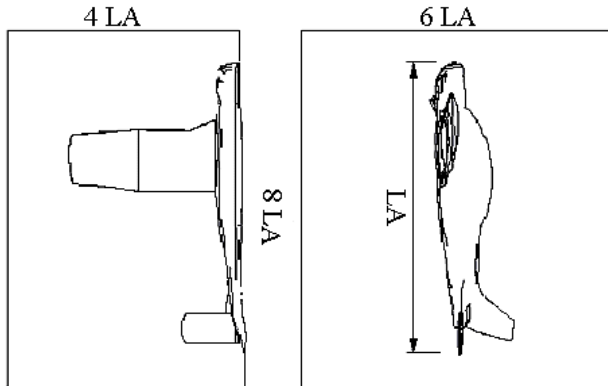


Figure 3. Complete airplane model. LA=Length of Airplane.

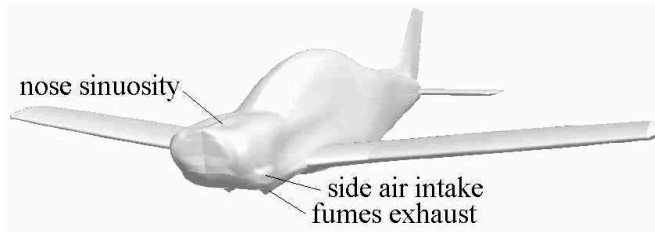


Figure 4. Final geometric model for the airplane.

#### 4 DESIGN AND CREATION OF THE MESHES

From the considered domain it was needed to generate meshes that as much fulfilled the requirements of the turbulence model (S-A) like the physical conditions of the flow. It was decided to use a mapped mesh (with only hexahedral and prismatic elements) that gives a faster convergence and generally, with better results. The more difficult part was in the meshing of the complex forms; for which reason it was needed to split the domain into regular blocks (prisms and quadrangles) that were easy to mesh. The advantage of this solution is to get a better mesh control and, when not using tetrahedral elements, fewer elements are needed, therefore, less computational cost and calculation time. In this way, blocks were meshed for the 3D models utilizing 92 blocks for the wing model and 512 for the complete airplane.

For the turbulence model (S-A), the mesh requirements are based on the near wall treatments. The options are the two-layer model (TLM) and wall-function model (WFM), the first type being used in the 2D model and both types being used for 3D models.

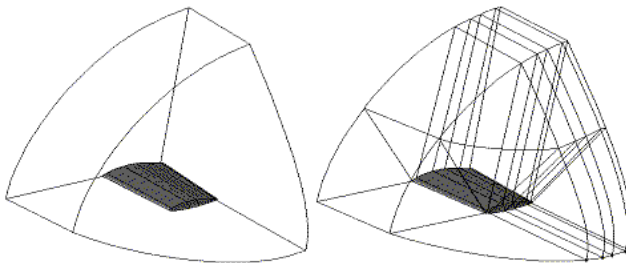


Figure 5. 3D Domain splitting example.

The difference between both models is in the adimensional parameter  $y^+$  at the surfaces. According to the S-A model, this must take a value near 1 (not greater than 5) for two-layer model and values near 30 for wall-function model, in other words, that the first model requires much more fine meshing but, according to its appraisal, it gives slightly better results than the WFM. Thus, the TLM was used for the lifting surfaces (wing and tail horizontal stabilizer) and WFM for the rest of the airplane. Finally, 8,700 cells were used for the airfoil model (2D), 270,000 for the wing model (figure 6) and just 320,000 for the complete airplane.

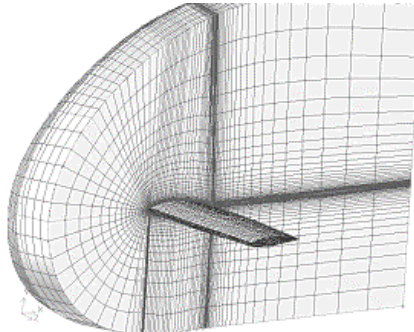


Figure 6. Mesh detail on the finite wing model.

## 5 SOLUTION CALCULATION

In this stage, it corresponds to choose the simulation parameters such as solver, physical models, air properties, boundary conditions settings, discretization scheme and convergence monitors. The solver used was the coupled / implicit (speed-up increasing<sup>3</sup>) / steady, where the coupled model although preferred for compressible flows ( $Mach > 0.3$ ), for this case at some flight conditions some important local effects of compressibility happen, such as for the maneuver condition ( $M 0.25$ ) and maximum load factor, where some local Mach numbers take values near 0.45.

The most relevant air properties, for this range of simulation speed, are the density and viscosity. For the first case, the ideal gas model was used (by the mentioned effects of compressibility) and the Sutherland Law as the viscosity model.

In the discretization schemes, the upwind schemes were used (first and second order) to reach the final solution. The other schemes (Power Law and QUICK) do not give substantial variations of the solution.

The solution was obtained in a personal computer (768 MB RAM, Pentium III® processor) lasting about a day by simulated case with 1,000 iterations each.

## 6 ANALYSIS OF THE FLOW AROUND THE AIRFOIL

The results for the 2D model showed excellent results emphasizing the lift curve as function of the angle of attack (figure 7), where the average difference with the experimental values is -3% and considering the results dispersion, the differences range is between -5 to 3%. For the drag and pressure coefficients distribution, a similar situation happens (figure 8), where the difference does not exceed 18%. In this way, it was possible to get the minimum requirements of mesh to obtain good results, being vital information for the generation of 3D models that can use minimum computational resources.

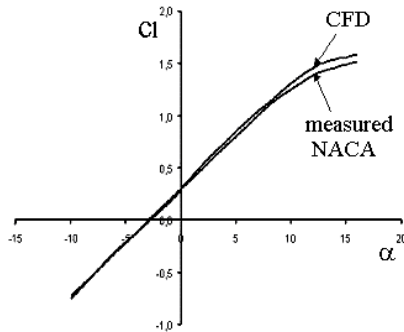


Figure 7. Lift curve comparison (NACA and CFD) for the airfoil NACA 65<sub>2</sub>-415.

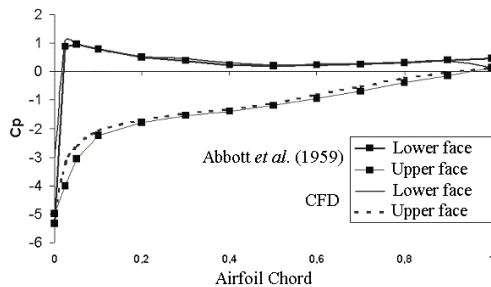


Figure 8. Pressure coefficients distributions ( $C_p$ ) for the airfoil NACA 65<sub>2</sub>-415 at  $\alpha=12^\circ$ .

## 7 ANALYSIS OF THE FLOW AROUND THE FINITE WING

The results for the finite wing are based on the lift distribution throughout the wing. The analyzed case is a twisted straight tapered wing with three section changes. These results were compared with some traditional methods for the lifting-line like Prandtl<sup>17</sup>, Anderson<sup>2</sup> and Rasmussen-Smith<sup>13</sup>. This comparison of results appears in table I as the wing lift coefficient for two different angles at the wing root (the wing root has an incidence angle of  $2^\circ$  with respect to airplane center-line), emphasizing that these methods are not able to predict the wing drag, but the induced drag. The CFD model, however, can predict this value and it has been included in table I.

	<i>Prandtl</i>	<i>Anderson</i>	<i>Rasmussen-Smith</i>	<i>CFD S-A</i>	
	$C_{L \text{ wing}}$	$C_{L \text{ wing}}$	$C_{L \text{ wing}}$	$C_{L \text{ wing}}$	$C_{D \text{ wing}}$
$\alpha = 2^\circ$	0,29	0,28	0,28	0,31	0,015
$\alpha = 14^\circ$	1,12	1,25	1,14	1,08	0,162

Table I. Comparison for the aerodynamics coefficients for the finite wing.

The best results are seen with the classic Prandtl theory, solved by the Glauert method<sup>15</sup>. This same conclusion appears comparing the lifting-line on the wing. In figure 9 is shown the comparison of section lift coefficient divided by the total lift of the wing, getting an average difference of 6%, with a probabilities range from 0,3% to 13%. In this way, the necessary mesh characteristics and FLUENT® capabilities have been discovered in order to get good results for the determination of aerodynamic loads on a flying airplane.

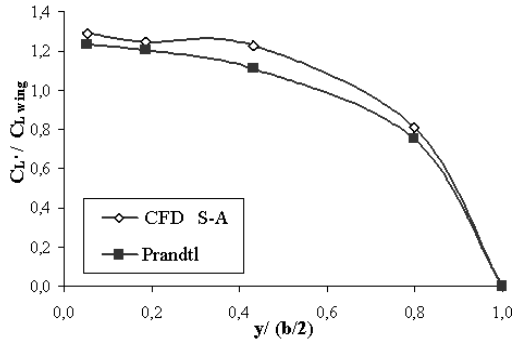


Figure 9. Comparison for the lifting distribution on the wing.

## 8 COMPLETE AIRPLANE RESULTS

Few referential values for the validation of the CFD results exist. For this reason, the results that the CFD model of the complete airplane gives must be subject to the uncertainty of results shown in the previous modeling stages.

In order to analyze the aerodynamic performance for the airplane, it is important to simulate significant conditions of flight such as low speed stall ( $M$  0.1 at maximum angle of attack), maneuver ( $M$  0.25,  $n=-3$  and 6) and dive ( $M$  0.37,  $n=-3$  and 6). In addition, it is of interest to see the effect of the aerodynamic loads in the main structures of the airplane, splitting it into 5 parts: nose, wing, main body, tail and tail cone (see fig. 10).

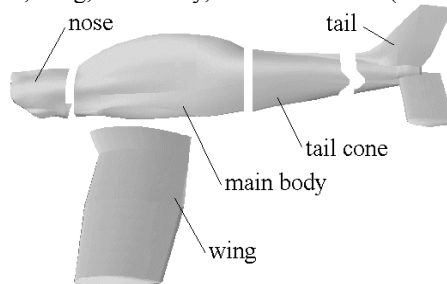


Figure 10. Main structures of the airplane.

The aerodynamic forces were divided by the projected surfaces: vertical projections for lift and frontal projections for drag values. The lift and drag shows the same facts: the load distributions on the different parts of the airplane, for the same angle of attack, are independent of the speed of flight. In the example, for the angle of attack of 2 degrees (at the wing-root) without the speed of flight mattering, the lift force on the wing will be 63% of the airplane lift and tail the only 15%. The circle graphs for the lift and drag distributions appear in figures 11 and 12, respectively.

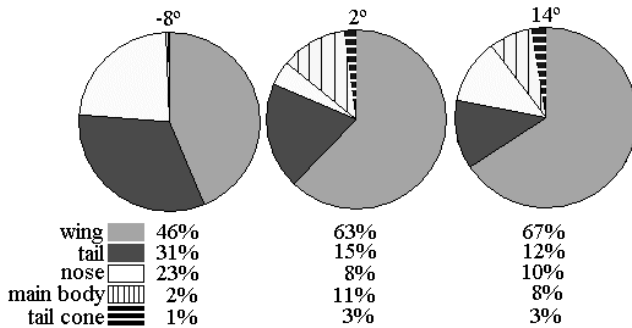


Figure 11. Lift distribution on the main structures of the airplane as function of the angle of attack.

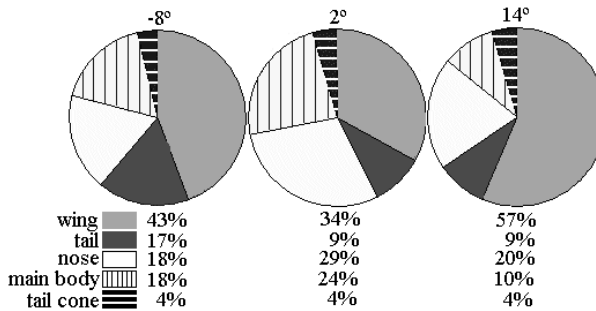


Figure 12. Drag distribution on the main structures of the airplane.

There, at low angle of attack (smaller drag), the greater contributor is the pressure drag, emphasizing the nose of the airplane as well as the empennage (particularly the vertical stabilizer because this is a kind of swept wing with high drag). The wing, on the other hand, that has an airfoil NACA 6-series, is designed to favor the laminar flow, that is to say, it gives low drag for low angles of attacks, so the wing is not, singularly, the greatest participant in the total drag of the airplane for those conditions. At high angles of attack (negative as positive) the importance of the wing in the drag increases as much due to the induced drag (proportional to the square of the lift) as by boundary layer separation that has begun to

happen.

Once the loads on the complete structure of the airplane had been determined, a graph of the load factor ( $L/W$ ) was made as a function of the angle of attack at the wing-root (figure 13), for the rank of speed that includes the dominion of flight (from  $M 0,1$  until  $M 0,37$ ).

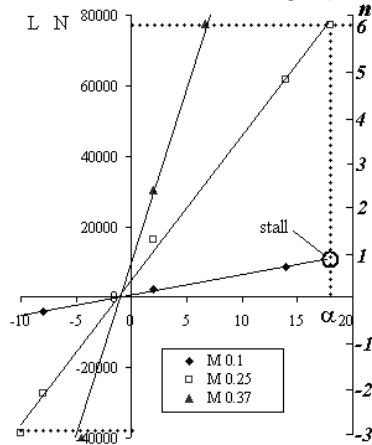


Figure 13. Airplane Lift force ( $L$ ) and Load Factor ( $n$ ) as function of the angle of attack ( $\alpha^\circ$ ) and speed of flight.

Thus, the flight dominion corresponds to the area locked up by the lines of  $M 0.37$  and  $M 0.1$ , including the linear tendencies. The dotted lines at  $n=6$  and  $n=-3$  correspond to the flight domain limits for the structural requests.

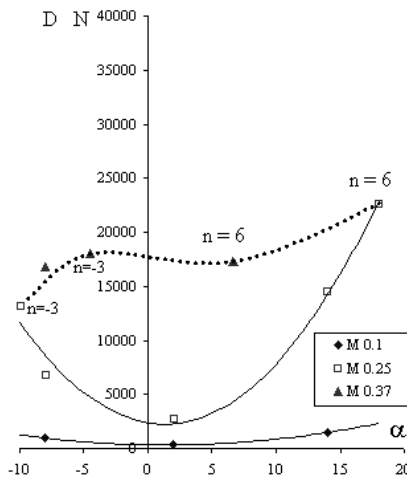


Figure 14. Airplane Drag force ( $N$ ) as function of the angle of attack ( $\alpha^\circ$ ) and speed of flight.

Figures 13 and 14 show the aerodynamic forces for the complete airplane based on the angle of attack at the wing-root. As validation of these values, very few experimental results exist. One of these values is the stall angle at Mach 0.1, that is to say, where the load factor  $n = 1$ . According to the flight measurements, this angle is  $17,26^\circ$  in wing-root and, as a result of the linear tendency of the curve for M 0.1 (figure 13), this value is near to  $18^\circ$ . Another comparable value is the drag for the maximum speed in horizontal flight (angle of  $2^\circ$  in the wing-root) or, as a pilot would say, “straight and leveled with maximum power”. This measured speed turned out to 160 knots (82 m/s or M 0.25) and corresponds to the maximum speed that can be reached with the maximum engine power (300 HP or 223.7 kW). If all this power is used, (100% propeller efficiency) the total drag for that condition is 2,728 N. According to the graph of figure 14, the drag calculated for the same flight conditions ( $n=1$  and Mach 0.25) is 2,064 N, that is to say, a difference of 32% with respect to the measured value. Obviously the measured drag value has not considered losses like the propeller efficiency that is normally high, near 90%<sup>10</sup>. On the other hand, this value (30%) is coherent with the expectations in the drag calculation, according to the one shown at “Computational geometric modeling” and indicates that the drag values of figure 14 must be amplified by this 30%.

Finally, the worst flight conditions need to be defined. Clearly, it must be in the maximum load factors zone, so the moment’s loads at the wing could explain it. In figure 15 are the moments curves for the bending and torsion with respect to the main spar (or beam) of the wing. The points for the flight conditions with maximum load factor ( $n = 6$ ) are shown in circles and squares.

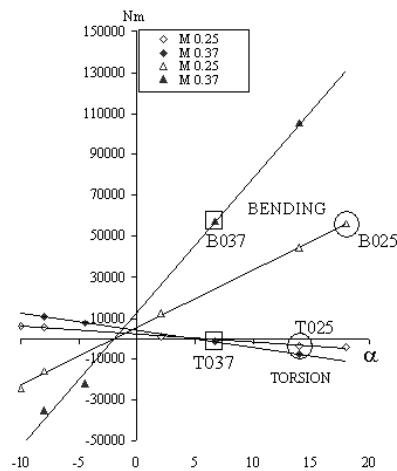


Figure 15. Bending and torsion moments by the wing external loads with respect to the main spar as function of the angle of attack.

The points B025 and B037 showed the critical bending points M 0.25 and M 0.37, respectively. With the same nomenclature appear the points in torsion for M 0.25 (point T025) and M 0.37 (point T037). Slightly it comes to appreciate that the T025 point has a greater value (negative) of the torsion than the T037, however the points B025 and B037 display very similar values. This is clearer in a table of data (Table II) where the values of the twist are compared with results calculated from models based on potential flow<sup>4</sup> and applied to the wing of this airplane<sup>16</sup>. There, the values of the twist for the potential flow model are higher than the CFD model, since in the first case, the entire flight load is supported by the wing, which results in exaggeration when appreciating the figures 11 and 12 of this work, appreciating the importance of calculating the aerodynamic loads from a complete structure model of the airplane.

Flight condition		CFD Model Complete airplane	Vega, 2001 Wing model
n	V m/s	Mt <sub>SPAR</sub> Nm	Mt <sub>SPAR</sub> Nm
6	M 0.25	T025 = -4,455	-11,617
6	M 0.37	T037 = -1,620	-6,806

Table II. Comparison of the torsion moment (twist) at the main spar of the wing.

## 9 CONCLUSIONS

After the results comparison (CFD and experimental or theoretical values), it have been possible to establish certain appreciations on aerodynamic performance of the airplane and the capacities of this CFD code in the aerodynamic simulation for this category of airplanes (less than 5,700 kg):

a) The complete structure model of the airplane, allowed establishing the critical flight condition according to where the maximum requests for the wing happen. This condition limit happens for the cruise speed of flight (Mach 0.25) and load factor equal to six, or angle of attack 18° at the wing-root. There it happens that the lift and drag forces, bending and twisting in the main spar of the wing are maximum, even greater than for the maximum flight speed (Mach 0.37). This condition can be predicted by semi-empirical analysis methods but the loads values are too high.

b) An assembly of graphs was developed that allows considering the maximum loads on the wing as a function of the speed of flight and the angle of attack (figures 13 to 15), showing that the loads are a linear function of the airplane angle of attack. From these graphs, the resulting loads can be obtained for other structural elements at intermediate flight conditions, different from the simulated conditions in this CFD model.

c) The airfoil results, as much as 3D results, did show excellent results. In the worst case, and considering the results dispersion, these differences would not exceed the range of  $\pm 20\%$  as a conservative way for all the aerodynamic loads. The best results obtained for the lifting was where the differences range did not exceed 13%.

d) Another important contribution that FLUENT® gives is the analysis of physical problems that cannot be calculated by traditional methods like the drag and the effects of boundary layer separation (stall), and that was still restricted to be obtained only at laboratories<sup>11</sup>. A great advantage of this tool, in the aerodynamic simulation, is the possibility of obtaining good quality results by an inexpensive way (processing in personal computer without the need of great parallel systems).

e) A different analysis topic constitutes the study of differences between the CFD values and the measured ones or by theoretical methods. It is seen as indispensable to have a procedure (like a sampling statistical method) that allows the establishing of your own range of differences for the numerical simulation. For this case the differences range was calculated from a normal distribution, meaning, for a probability of 98%, the differences range is between the average value  $\pm 2\sigma$ , as a conservative way for the error estimation. A great statistical analysis of CFD results is shown in the references<sup>14</sup>.

## 10 REFERENCES

- [1] Abbott I. H., and Von Doenhoff A. E., *Theory of Wing Sections*, Dover Publications Inc, 1959.
- [2] Anderson J. D. Jr., *Fundamentals of Aerodynamics*, McGraw-Hill Inc, 1991.
- [3] Becker K., Aumann P., Barnewitz H., Schwarten H., Heinrich R., Roll B., Galle M., Kroll N., Gerhold Th., Schwamborn D., Franke M., MEGAFLOW: Parallel complete aircraft CFD, *Parallel Computing*, Vol. 27 No 4 (2001) pp. 415-440.
- [4] Diederich F. W., A Simple Approximate Method for Calculating Spanwise Lift Distributions and Aerodynamic Influence Coefficients at Subsonic Speeds, Langley Aeronautical Laboratory, *NACA Technical Note* N° 2751, 1952.
- [5] Federal Aviation Administration –FAA, *Federal Aviation Regulations, Part 23 – Airworthiness Standards: Normal, Utility, Acrobatic And Commuter Category Airplanes*, 1991.
- [6] FLUENT Inc., *FLUENT® User's Guide - Release 5.3*, 1999.
- [7] Goett H. J. and Bullivant W. K., Tests of NACA 0009, 0012, and 0018 airfoils in the full-scale tunnel, *NACA Report 647*, 1939.
- [8] Köck R., Aplicación del Código FLUENT® en el Cálculo de Coeficientes Aerodinámicos para un Perfil NACA 65<sub>2</sub>-415. *2nd Aerospace Engineering Meeting*, Aeronautical Polytechnic Academy FACH. Santiago, Chile (2000).
- [9] Madariaga, R., Análisis numérico del flujo alrededor del empenaje de un avión, *Mechanical Engineering Project*. Department of Mechanical Engineering, University of Concepción, Concepción, Chile, 2001.
- [10] McCormick B. W., *Aerodynamics, Aeronautics, and Flight Mechanics*, John Wiley & Sons, 1979.
- [11] Pátek Z. and Smrcek L., Aerodynamics characteristics of multi-surface aircraft configurations, *Journal of Aircraft Design*, Vol 2 No 4 (1999) pp. 191-206.

- [12] Quinn J., Summary of Drag Characteristics of Practical-Construction Wing Sections, *NACA Report No 910*, 1948.
- [13] Rasmussen M. and Smith D., Lifting-Line Theory for Arbitrarily Shaped Wings, *Journal of Aircraft*, Vol 36 No 2 (1999) pp. 340-348.
- [14] Sturek W. and Taylor M., Statistical Analysis of CFD Results for Missile Surface Pressures, Army Research Laboratory - *AIAA 18<sup>th</sup> Applied Aerodynamic Conference and Exhibit*, Denver, CO, (2001).
- [15] Thwaites B., *Fluid Motion Memoirs. Incompressible Aerodynamics*, Oxford University Press, 1960.
- [16] Vega M., Diseño asistido por computador de estructuras aeronáuticas mediante criterios de tolerancia al daño, *M. Sc. Thesis*, Department of Mechanical Engineering, University of Concepción, Concepción, Chile, 2001.
- [17] Von Mises R., *Theory of Flight*, Dover Publications, 1959.